Supporting Information for:

Growth kinetics and size distribution dynamics of viscous secondary organic aerosol

Rahul A. Zaveri[1], John E. Shilling[1], Alla Zelenyuk[2], Jiumeng Liu[1], David M. Bell[2,§], Emma L. D'Ambro[3,4], Cassandra J. Gaston[3,†], Joel A. Thornton[3,4], Alexander Laskin[5,‡], Peng Lin[5,‡], Jacqueline Wilson[2], Richard C. Easter[1], Jian Wang[6], Allan K. Bertram[7], Scot T. Martin[8,9], John H. Seinfeld[10,11], and Douglas R. Worsnop[12]*

[1]Atmospheric Sciences and Global Change Division, Pacific Northwest National Laboratory, Richland, WA 99352, USA

[2]Physical Sciences Division, Pacific Northwest National Laboratory, Richland, WA 99352, USA

[3]Department of Atmospheric Sciences, University of Washington, Seattle, WA 98195, USA

[4]Department of Chemistry, University of Washington, Seattle, WA 98195, USA

[5]William R. Wiley Environmental Molecular Sciences Laboratory, Pacific Northwest National Laboratory, Richland, WA 99352, USA

[6]Environmental and Climate Sciences Department, Brookhaven National Laboratory, Upton, NY 11973, USA

[7]Department of Chemistry, University of British Columbia, Vancouver, BC V6T 1Z1, Canada

[8]John A. Paulson School of Engineering and Applied Sciences, Harvard University, Cambridge, MA 02138, USA

[9]Department of Earth and Planetary Sciences, Harvard University, Cambridge, MA 02138, USA

[10]Division of Chemistry and Chemical Engineering, California Institute of Technology, Pasadena, CA 91125, USA

[11]Division of Engineering and Applied Science, California Institute of Technology, Pasadena, CA 91125, USA

[12]Center for Aerosol and Cloud Chemistry, Aerodyne Research, Billerica, MA 01821, USA

*Correspondence to: R. A. Zaveri (rahul.zaveri@pnnl.gov)

This file includes:

MATERIALS AND METHODS

Instruments

FIGAERO HR-ToF-CIMS

The Filter Inlet for Gases and AEROsols has been described in detail previously[1]. The FIGAERO was coupled to a high-resolution time of flight chemical ionization mass spectrometer (HR-ToF-CIMS) using Iodide adduct ionization also described in detail previously[2]. Briefly, the FIGAERO is an inlet manifold that allowed for measurement of both gas- and particle-phase molecular composition with approximately hourly resolution. To collect particles, chamber air was drawn through a 0.635 cm OD stainless steel tube at 2.5 slpm across a Teflon filter (Zefluor® 24 mm diameter, 2.0 μm pore size, Pall Corp.) for 25 minutes. Through a separate inlet, chamber air was simultaneously sampled at 12 slpm through a 1.9 cm OD, 1.1 m long PTFE tube for gas-phase analysis. The gas-phase analysis required sub-sampling the gas-phase inlet chamber output after dilution to maintain linearity of response in the chemical ionization. After a particle collection period, the filter was actuated to a location downstream of an ultra-high purity (UHP) N_2 source and immediately upstream of an orifice into the HR-ToF-CIMS. UHP N_2, continually passed across the filter at 2.5 slpm, was heated at a rate of 10 or 15 °C min^{-1} to 200 °C for a temperature-programed thermal desorption and then kept at 200 °C for the remainder of the desorption time (40 min total desorption time). The temperature axis of the FIGAERO thermograms is calibrated with compounds having known enthalpies of sublimation[1]. It has been shown that pure compounds, or mixtures of non-interacting compounds, have consistent thermogram shapes throughout time and reach a maximum signal at characteristic

temperature (T_{max}) which can be related to their enthalpies of sublimation and therefore sub-cooled pure component vapor pressures[1]. In this way, the T_{max} of detected compounds can be used to estimate their C* at ambient conditions even if the structure is unknown.

Nano-DESI-HRMS

A custom-built Nanospray Desorption Electrospray Ionization (Nano-DESI) source coupled to a high resolution LTQ-Orbitrap mass spectrometer (Thermo Electron, Bremen, Germany) was used to analyze SOA filter samples. Briefly, the sample was positioned on a computer-controlled XYZ stage and brought in contact with the Nano-DESI probe, which was assembled using two fused silica capillaries (50 × 193 µm, ID × OD, Polymicro Technologies, L.L.C., Phoenix). The solvent (70/30%, acetonitrile/water) was infused using a syringe pump at a flow rate of 0.3-1µL min^{-1} that was matched to the self-aspiration rate of the nanospray capillary[3]. Typical experimental conditions were: spray voltage of 3.5kV, 250 °C temperature of the heated capillary, and the mass spectrometer was operated in the positive ion mode with a resolving power of $m/\Delta m = 10^5$ at m/z 400. The instrument was regularly calibrated using a standard calibration MSCAL 5 mixture (Sigma-Aldrich, Inc.). Mass spectral features with a minimum signal-to-noise ratio of 3 were extracted from the averaged mass spectra of both solvent background and sample using Decon 2LS software[4] (http://omics.pnl.gov/software/decontools-decon2ls). Data processing was performed using a suite of Microsoft Excel macros, including background subtraction, first and second-order mass defect analysis[5,6]. Formula assignments with constraints of C: 1–40, H: 2–80, O: 0–35, Na: 0–1 were performed using the Molecular Formula Calculator (https://nationalmaglab.org/user-facilities/icr/icr-software) for ions of the type $[M+H]^+$ or $[M+Na]^+$ with a tolerance of 2 ppm of mass measurement error.

Single particle mass spectrometer miniSPLAT

Single particle mass spectrometer, miniSPLAT, was used for real-time measurements of particle vacuum aerodynamic diameter (D_{va}), density, shape, composition, and evaporation kinetics. A detailed description of miniSPLAT and its use for the measurement of particle properties and evaporation kinetics are provided elsewhere[7-10]. Briefly, individual aerosol particles enter miniSPLAT through an aerodynamic lens inlet[11] and detected by light scattering in two optical stages 10.9 cm apart. The time it takes the particles to pass between the two optical stages yields particle velocity, which is used to calculate particle D_{va} with precision and accuracy of ±0.5%. The dual particle detection is also used to generate a trigger for the excimer laser, to generate positive and negative ions and acquire mass spectra of individual particles. Measurements conducted on size-selected particles provide information on particle shape, precise density (±0.5%), and evaporation kinetics.

Box Models

In this study, we used a multi-layer particle box model and a sectional aerosol model MOSAIC to separately interpret aerosol evaporation kinetics and growth kinetics, respectively. The multi-layer particle model can more accurately simulate than MOSAIC the effects of bulk diffusion on both evaporation and growth kinetics of a particle. Hence we use it to interpret evaporation kinetics of single particles. However, the multi-layer model is essentially a single particle model and is not ideally suited for simulating dynamics of an aerosol size distribution. Hence we use the sectional MOSAIC model to interpret the growth kinetics of the bimodal aerosol size distribution.

Multi-layer Particle Box Model

The multi-layer particle box model divides a single spherical particle into 200 concentric layers and explicitly simulates mass transfer of multiple compounds from the particle by taking into account compound volatility (C*), gas-phase diffusivity (D_g), interfacial mass accommodation (α), effective intra-particle bulk diffusivity (D_b), and reversible particle-phase reactions[12]. A finite-difference method is used to calculate temporal evolution of condensed species concentrations in each layer. As particles shrink (or grow) with time, the boundary radii of the layers decrease (or increase). To account for this, aerosol species mass is transferred between layers after each diffusion time-step to maintain uniform layer thickness. As an example, consider a 40 nm radius particle with only 4 layers, so the layer boundary radii are 10, 20, 30, and 40 nm. If the particle shrinks to 36 nm, the boundary radii change to 9, 18, 27, and 36 nm. In the diffusion and mass-transfer time-step calculations, the aerosol mass between 36 and 40 nm in the outermost layer (layer 4) is transferred to the gas phase. After that, aerosol mass between 9 and 10 nm radius is transferred from layer 1 to layer 2; aerosol mass between 18 and 20 nm is transferred from layer 2 to 3; and aerosol mass between 27 and 30 nm is transferred from layer 3 to 4. Gas-particle mass transfer is calculated using bulk gas concentrations and Fuchs-Sutugin[13] mass transfer coefficients. Model inputs include initial particle size (D_p) and composition along with D_g (assumed at 0.05 $cm^2\ s^{-1}$), D_b, α, and C* of all of evaporating compounds. The multi-layer particle model is conceptually similar to the KM-GAP model[14], except it does not include reversible adsorption at particle surfaces or heat transfer.

MOSAIC

The sectional aerosol box-model Model for Simulating Aerosol Interactions and Chemistry (MOSAIC)[15] dynamically partitions multiple compounds to all particle size bins by taking into

account compound volatility, gas-phase diffusion, interfacial mass accommodation, intra-particle bulk diffusion, and reversible particle-phase reactions. The thermodynamic driving force for mass transfer is based on Raoult's law. Bulk diffusion is treated using a combination of (1) an analytical quasi-steady-state treatment for the diffusion–reaction process within the particle phase for fast-reacting organic compounds such that the timescales for their particle-phase concentrations to reach quasi-steady state are shorter than 1 min, and (2) a two-film theory approach for slow- and non-reacting organic compounds. The logarithmically spaced bin structure and the number of bins used in the MOSAIC were same as that of the particle size distribution data provided the SMPS. Transfer of particles between bins due to growth or shrinkage was calculated using a two-moment approach. Coagulation was accounted for in the simulations.

Table S1. Summary of Aerosol Growth Experiments.

	Initial (at the beginning of Stage 2)				After some growth in Stage 2				
	Aitken Mode		Accumulation Mode			Aitken Mode		Accumulation Mode	
Expt.	D_p (nm)	SOA ($\mu g\ m^{-3}$)	D_p (nm)	SOA ($\mu g\ m^{-3}$)	Δt (min)	D_p (nm)	SOA[a] ($\mu g\ m^{-3}$)	D_p (nm)	SOA[a] ($\mu g\ m^{-3}$)
1	41.4	0	209.1	7.0	60	82.0	0.45	216.7	8.48
2	37.2	0	269.0	12.5	32	73.7	2.03	299.6	15.0

[a]Corrected for particle wall loss.

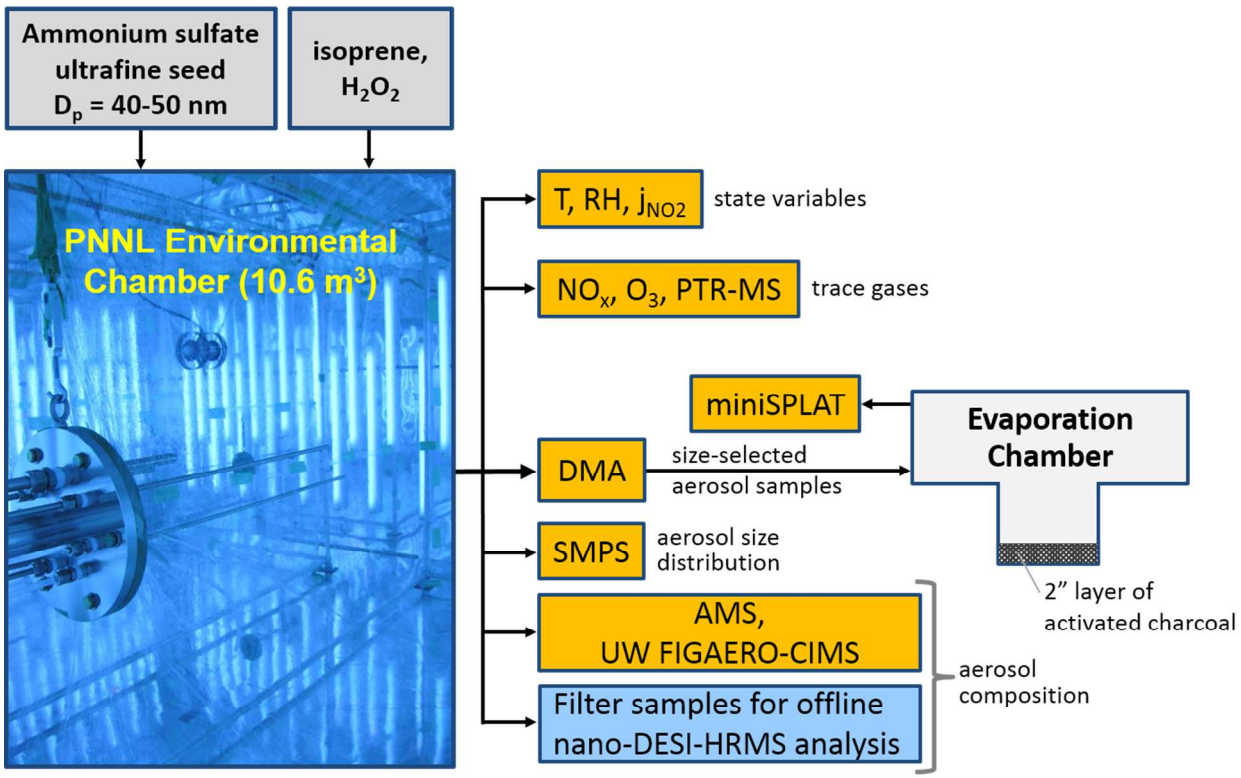

Figure S1. Schematic of experiment set up. Aerosol growth kinetics experiments were conducted in 10.6 m^3 FEP Teflon environmental chamber at Pacific Northwest National Laboratory. The chamber was run in the so-called batch mode where reactants were added to the chamber in discrete quantities. Instruments shown with orange background measured in real time (i.e., online) the state variables, trace gases, particle size distribution, and aerosol composition. Filter samples were collected at the end of the experiment for offline chemical analysis. Size-selected SOA particles formed in the environmental chamber were transferred at various stages of the experiment to separate small chambers to study their evaporation kinetics under dry conditions and room temperature.

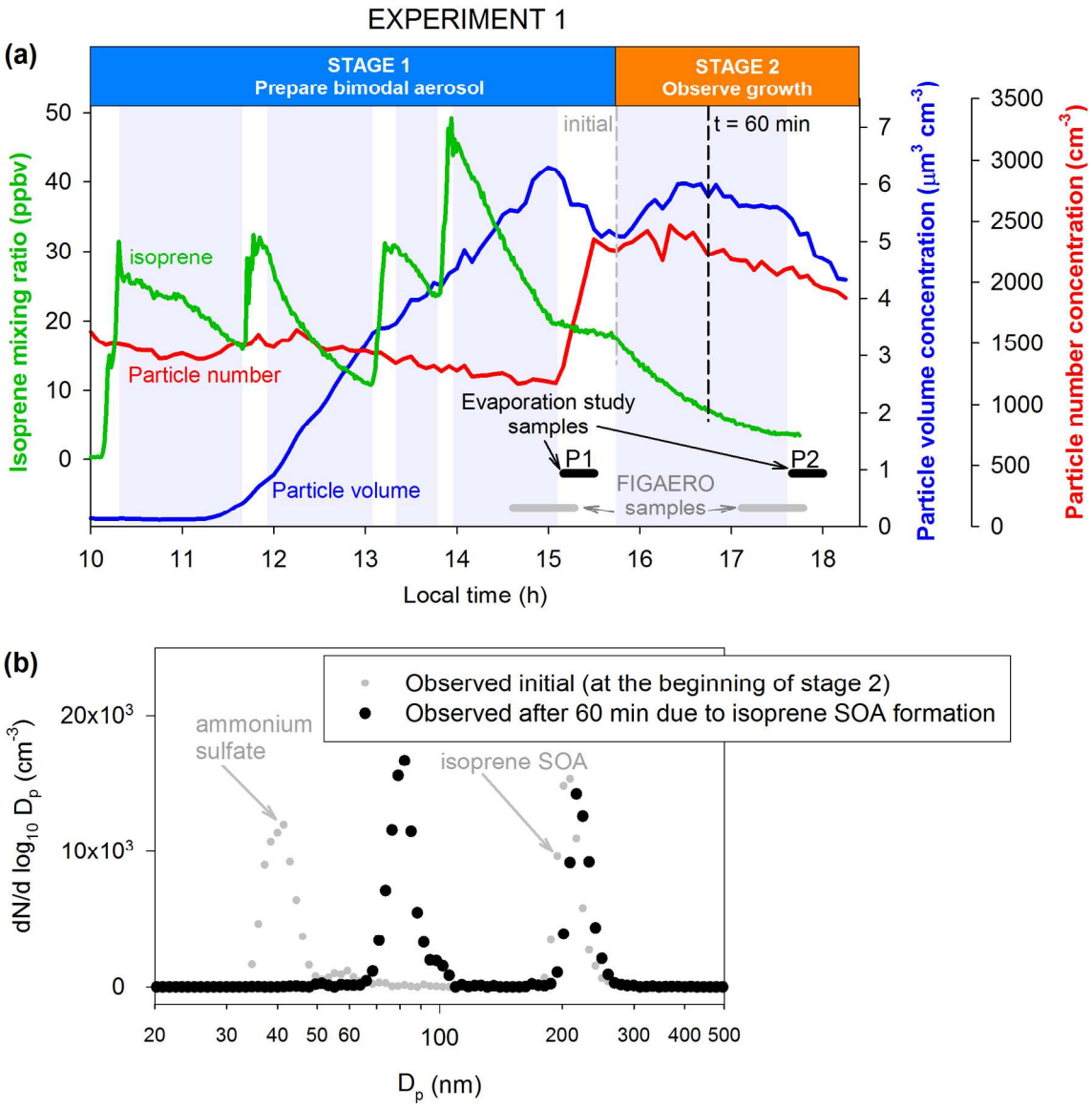

Figure S2. Time evolution of key variables in Experiment 1. (a) Evolution of isoprene, particle volume and number concentrations in the large environmental chamber as a function of time. Stage 1 represents the part of the experiment during which a bimodal aerosol consisting of Aitken mode ammonium sulfate particles (mode diameter ~40 nm) and accumulation mode isoprene SOA particles (mode diameter ~230 nm) was prepared in the chamber. The SOA mass concentration at the end of Stage 1 was at atmospherically relevant level (~7 μg m^{-3}). Stage 2 represents the part of the experiment during which this bimodal aerosol was allowed to grow due to additional isoprene SOA formation. The collection periods of samples by FIGAERO-CIMS and for evaporation study are indicated with gray and black horizontal lines, respectively. The light blue shading indicates the periods when the UV lights in the chamber were turned on. The gray and black vertical dashed lines represent the conditions at the beginning of Stage 2 and after 60 min, respectively. The corresponding aerosol size distributions are shown in (b).

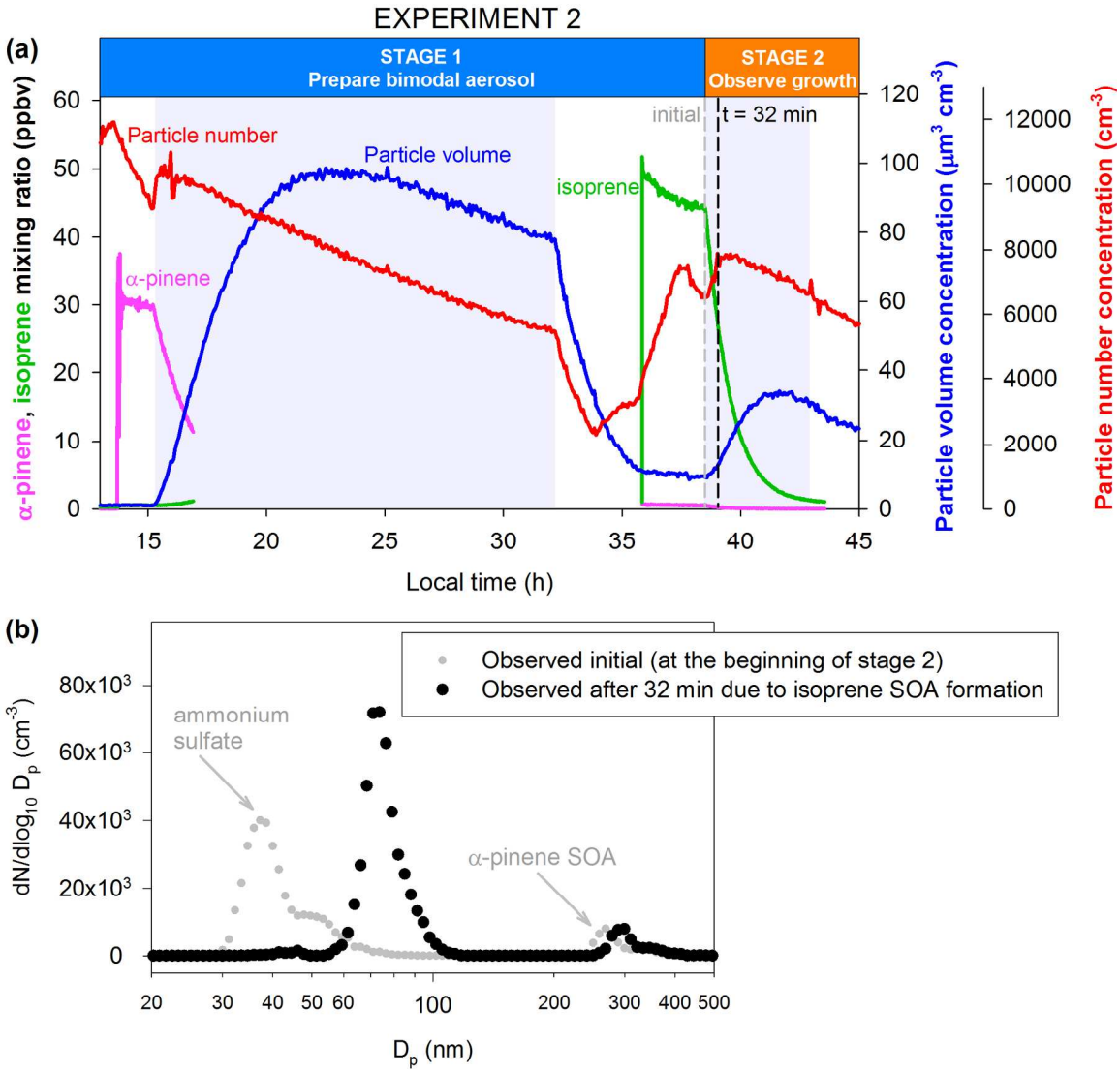

Figure S3. Time evolution of key variables in Experiment 2. (a) Evolution of α-pinene, isoprene, particle volume and number concentrations in the large environmental chamber as a function of time. In Stage 1, a bimodal aerosol consisting of Aitken mode ammonium sulfate particles (mode diameter ~40 nm) and accumulation mode α-pinene SOA particles (mode diameter ~270 nm) was prepared in the chamber. The light blue shading indicates the periods when the UV lights in the chamber were turned on. The rapid decrease in the particle number and volume concentrations seen after turning the UV lights off in Stage 1 was due to deliberate dilution of chamber air with clean air to adjust the particle concentration to the desired level. Aitken mode particles and isoprene are injected into the chamber toward the end of Stage 1. In Stage 2, the bimodal aerosol was allowed to grow due to isoprene SOA formation. The gray and black vertical dashed lines represent the conditions at the beginning of Stage 2 and after 32 min, respectively. The corresponding aerosol size distributions are shown in (b).

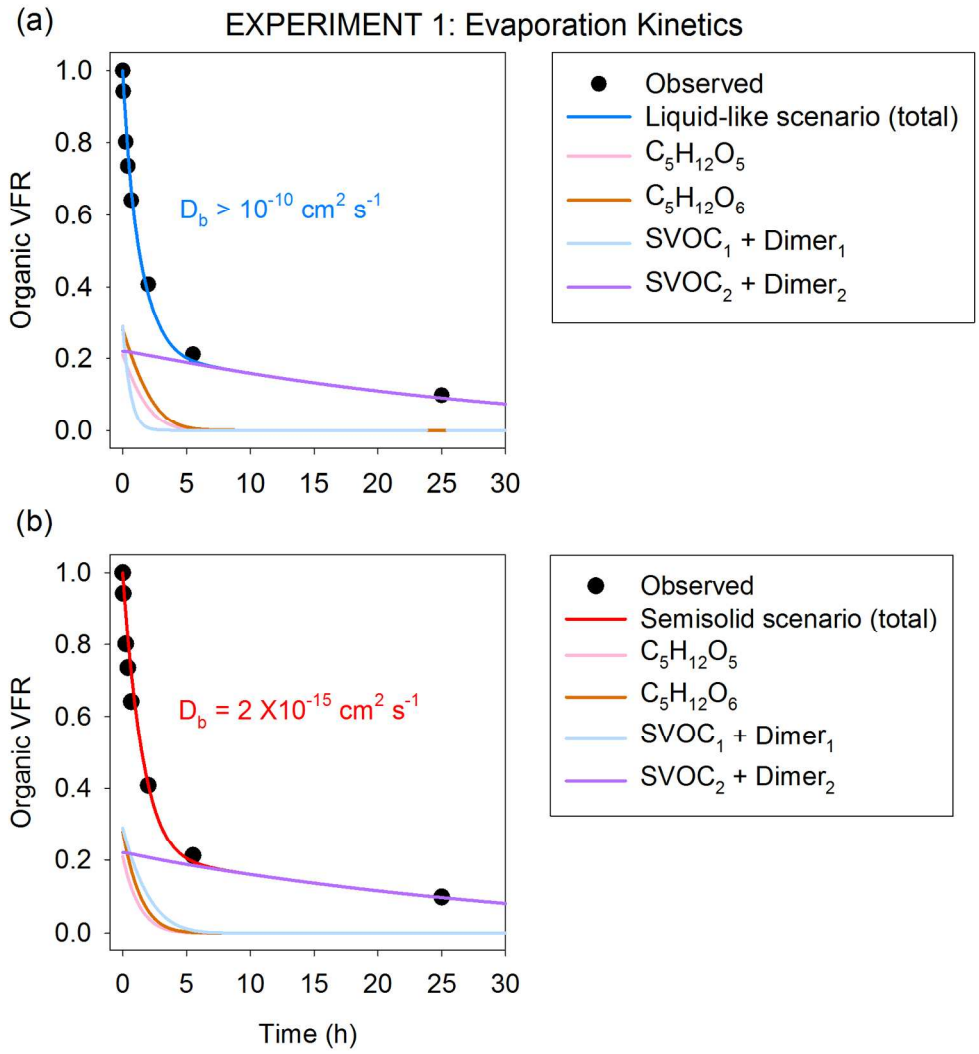

Figure S4. Observed and modeled evaporation kinetics for Experiment 1. Organic volume fraction remaining (VFR) curves are shown for the total particle and individual compounds for the accumulation mode isoprene SOA samples "P2" taken from the environmental chamber during Stage 2. (a) Liquid-like scenario. (b) Semisolid scenario. The evaporation of $SVOC_2$ is largely controlled by the relatively slow decomposition of $Dimer_2$ (timescale ~1000 min). In contrast, the evaporation curve of $SVOC_1$, which is produced from relatively fast decomposition of $Dimer_1$ (timescale ~30 min), is quite different for the liquid-like and semisolid scenarios due to different particle-phase diffusivities. The evaporation curves of the relatively less volatile $C_5H_{12}O_5$ and $C_5H_{12}O_6$ are somewhat similar for the liquid-like and semisolid scenarios, although subtle differences are seen due to different diffusivities.

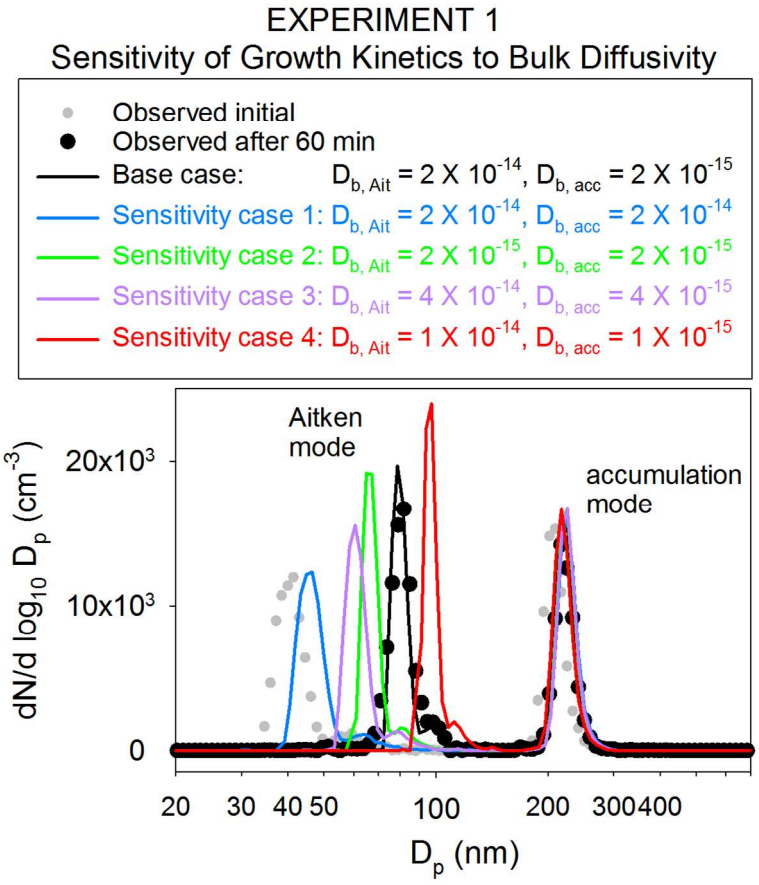

Figure S5. Sensitivity of growth kinetics to the prescribed bulk diffusivity values (cm^2 s^{-1}) for the Aitken mode ($D_{b, Ait}$) and accumulation mode ($D_{b, acc}$) in Experiment 1. Base case D_b values are the same as the semisolid scenario shown in Figure 4. As with the base case, the total amounts of SOA formed in each sensitivity case are constrained to the wall-loss corrected value of 1.93 µg m^{-3} observed after 60 min. In sensitivity case 1, D_b values for both modes are set at 2×10^{-14} cm^2 s^{-1}. In sensitivity case 2, D_b values for both modes are set at 2×10^{-15} cm^2 s^{-1}. In sensitivity case 3, D_b values for both modes are factor of 2 higher than their respective base case values. In sensitivity case 4, D_b values for both modes are factor of 2 lower than their respective base case values. A higher than base case $D_{b, acc}$ in sensitivity cases 1 and 3 while a lower than base case $D_{b, Ait}$ in sensitivity case 2 appreciably slows down the growth of the Aitken mode. In contrast, a lower than base case $D_{b, acc}$ in sensitivity case 4 over predicts the growth of the Aitken mode.

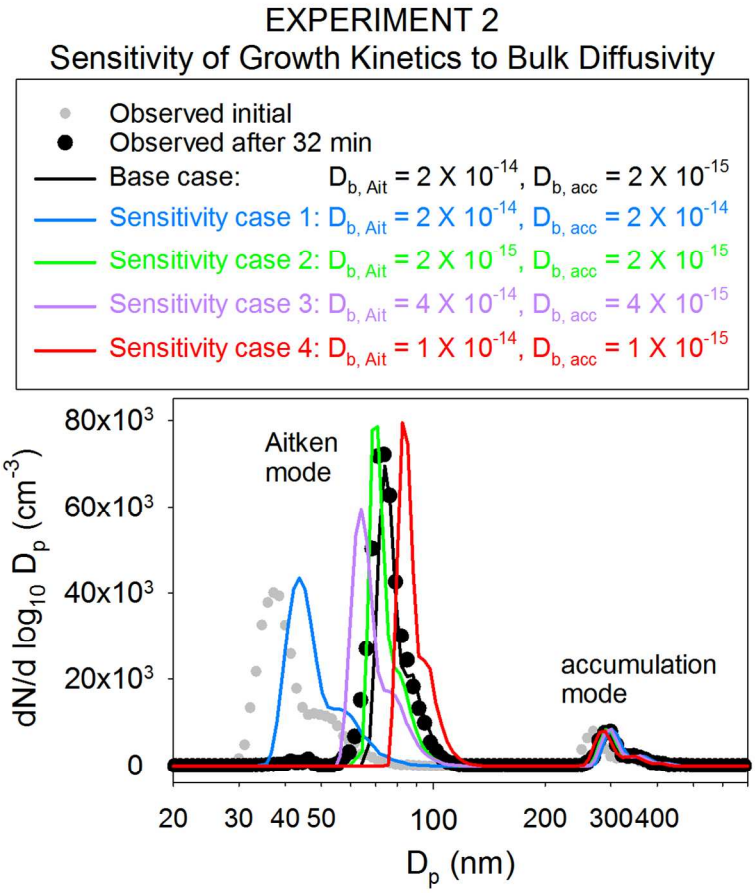

Figure S6. Sensitivity of growth kinetics to the prescribed bulk diffusivity values (cm^2 s^{-1}) for the Aitken mode ($D_{b, Ait}$) and accumulation mode ($D_{b, acc}$) in Experiment 2. Base case D_b values are the same as the semisolid scenario shown in Figure 5. As with the base case, the total amounts of SOA formed in each sensitivity case are constrained to the wall-loss corrected value of 4.53 µg m^{-3} observed after 32 min. In sensitivity case 1, D_b values for both modes are set at 2×10^{-14} cm^2 s^{-1}. In sensitivity case 2, D_b values for both modes are set at 2×10^{-15} cm^2 s^{-1}. In sensitivity case 3, D_b values for both modes are factor of 2 higher than their respective base case values. In sensitivity case 4, D_b values for both modes are factor of 2 lower than their respective base case values. A higher than base case $D_{b, acc}$ in sensitivity cases 1 and 3 while a lower than base case $D_{b, Ait}$ in sensitivity case 2 slows down the growth of the Aitken mode. In contrast, a lower than base case $D_{b, acc}$ in sensitivity case 4 over predicts the growth of the Aitken mode.

References

(1) Lopez-Hilfiker, F. D.; Mohr, C.; Ehn, M.; Rubach, F.; Kleist, E.; Wildt, J.; Mentel, Th. F.; Lutz, A.; Hallquist, M.; Worsnop, D.; Thornton, J. A. A novel method for online analysis of gas and particle composition: description and evaluation of a Filter Inlet for Gases and AEROsols (FIGAERO). *Atmos. Meas. Tech.* **2014**, 7 (4), 983-1001.

(2) Lee, B. H.; Lopez-Hilfiker, F. D.; Mohr, C.; Kurten, T.; Worsnop, D. R.; Thornton, J. A. An Iodide-Adduct High-Resolution Time-of-Flight Chemical-Ionization Mass Spectrometer: Application to Atmospheric Inorganic and Organic Compounds. *Environ. Sci. Technol.* **2014**, 48 (11), 6309−6317.

(3) Roach, P. J.; Laskin, J.; Laskin, A. Nanospray desorption electrospray ionization: an ambient method for liquid-extraction surface sampling in mass spectrometry. *Analyst* **2010**, 135, 2233-2236.

(4) Jaitly, N.; Mayampurath, A.; Littlefield, K.; Adkins, J. N.; Anderson, G. A.; Smith, R. D. Decon2LS: An open-source software package for automated processing and visualization of high resolution mass spectrometry data. *BMC Bioinformatics* **2009**, 10, 87.

(5) Eckert, P. A.; Roach, P. J.; Laskin, A.; Laskin, J. Chemical characterization of crude petroleum using nanospray desorption electrospray ionization coupled with high-resolution mass spectrometry. *Anal. Chem.* **2012**, 84, 1517-1525.

(6) Roach, P. J.; Laskin, J.; Laskin. A. higher-order mass defect analysis for mass spectra of complex organic mixtures. *Anal. Chem.* **2011**, 83, 4924-4929.

(7) Vaden, T. D.; Imre, D.; Beránek, J.; Shrivastava, M.; Zelenyuk, A. Evaporation kinetics and phase of laboratory and ambient secondary organic aerosol. *Proc. Nat. Acad. Sci. USA* **2011**, 108 (6), 2190-2195.

(8) Wilson, J.; Imre, D.; Beránek, J.; Shrivastava, M; Zelenyuk, A. Evaporation kinetics of laboratory-generated secondary organic aerosols at elevated relative humidity. *Environ. Sci. Technol.* **2015**, 49 (1), 243-249.

(9) Zelenyuk A, Yang J, Song C, Zaveri RA, Imre D (2008) “Depth-profiling” and quantitative characterization of the size, composition, shape, density, and morphology of fine particles with SPLAT, a single-particle mass spectrometer. J Phys Chem A, 112(4):669–677.

(10) Zelenyuk, A.; Imre, D.; Wilson, J.; Zhang, Z.; Wang, J.; Mueller, K. Airborne single particle mass spectrometers (SPLAT II & miniSPLAT) and new software for data visualization and analysis in a geo-spatial context. *J. Am. Soc. Mass Spec.* **2015**, 26, 257-270.

(11) Vaden, T. D., Imre, D., Beranek, J. and Zelenyuk, A. (2011). Extending the Capabilities of Single Particle Mass Spectrometry: I. Measurements of Aerosol Number Concentration, Size Distribution, and Asphericity. *Aerosol Science and Technology* 45:113-124.

(12) Zaveri, R. A.; Easter, R. C.; Shilling, J. E.; Seinfeld, J. H. Modeling kinetic partitioning of secondary organic aerosol and size distribution dynamics: representing effects of volatility, phase state, and particle-phase reaction. *Atmos. Chem. Phys.* **2014**, 14, 5153-5181.

(13) Fuchs, N. A.; Sutugin, A. G. (1971), High-dispersed aerosols, in Topics in Current Aerosol Research (Part 2), edited by G. M. Hidy and J. R. Brock, pp. 1 –200, Elsevier, New York.

(14) Shiraiwa, M.; Pfrang, C.; Koop, T.; Pöschl, U. Kinetic multilayer model of gas-particle interactions in aerosols and clouds (KM-GAP): linking condensation, evaporation, and chemical reactions of organics, oxidants and water. *Atmos. Chem. Phys.* **2012**, 12, 2777-2794.

(15) Zaveri, R. A.; Easter, R. C.; Fast, J. D.; Peters, L. K. Model for Simulating Aerosol Interactions and Chemistry (MOSAIC). *J. Geophys. Res.* **2008**, 113, D13204.